

# Characterizing Sub-THz MIMO Channels in Practice: a Novel Channel Sounder with Absolute Time Reference

Duschia Bodet\*, Phuc Dinh\*, Milica Stojanovic\*, Joerg Widmer<sup>†</sup>, Dimitrios Koutsonikolas\*, Josep Miquel Jornet\*

\*Department of Electrical and Computer Engineering

Northeastern University, Boston, MA, USA E-mail: {bodet.d,dinh.p,m.stojanovic,d.koutsonikolas,jmjornet}@northeastern.edu

<sup>†</sup>IMDEA Networks, Madrid, Spain E-mail: joerg.widmer@imdea.org

**Abstract**—Multiple-Input Multiple-Output (MIMO) systems have been presented for Terahertz (THz) communications to combat high path loss and enable Terabit-per-second (Tbps) links. The lack of experimental MIMO channel measurements, however, has restricted the majority of THz MIMO work to the theoretical realm. This paper presents a novel, first-of-its-kind correlation-based MIMO channel sounder with a timing reference for sub-THz communications, which enables broadband, long-range, and time-varying channel characterization of MIMO systems. Preliminary results from a conference room setting show that 28.5% of the tested scenarios can support spatial multiplexing, and even with beamforming, the capacity outperforms the SISO cases substantially.

**Index Terms**—Terahertz (THz), MIMO, channel sounding, experimental results, experimental platform

## I. INTRODUCTION

Terahertz (THz) communication systems have attracted significant interest in recent years, owing to their potential for ultra-high-speed wireless data transmission and the unique features of THz frequency bands. These characteristics include vast unlicensed spectrum and ultra-wide bandwidth, which makes the THz band a promising candidate for meeting the ever-increasing demands of wireless communication networks, particularly in beyond-5G and 6G applications. The increased available bandwidth alone, however, will not be enough to unlock the Terabit-per-second (Tbps) links promised for 6G applications. In order to reach Tbps link speeds with a reasonable amount of bandwidth (i.e., less than 50 GHz), systems will be required to use spatially multiplexed multiple-input multiple-output (MIMO) channels [1].

However, the research community currently lacks sufficient experimental channel measurements to inform models for THz MIMO channels. Many single-input single-output (SISO) channel sounders exist for (sub-)THz frequencies [2], but to characterize the capacity of a multiple-antenna system and the channel's ability to support spatial multiplexing, MIMO

channel sounders are needed. Although there are some experimental THz MIMO channel sounders, they are either VNA-based [3], [4] or are correlation-based and lack an absolute time reference [5]. VNA-based channel sounders are distance-limited and are not able to capture broadband, time-varying channel characteristics. Correlation-based THz channel sounders generally find the angle-of-arrival information by capturing signals at different angles using directional antennas. However, without an absolute timing reference, it is impossible to truly distinguish whether the received signal is part of the line-of-sight (LoS) component or a multi-path component. Additionally, it is impossible to tell if signals arriving at different angles arrive at sufficiently different times to improve the channel orthogonality.

In this paper, we present a first-of-its-kind broadband experimental platform to help bridge the gap between theoretical advancements and real-world deployment. Our key considerations include (a) accurately emulating THz MIMO channel conditions, (b) over a large bandwidth (c) in a realistic environment. Our method allows us to fully characterize the sub-THz MIMO channel in a given environment, including the MIMO channel capacity and the channel's ability to support spatial multiplexing.

The contributions of this work are as follows:

- We develop the first-of-its-kind MIMO sub-THz correlation-based channel sounding system operating over 20 GHz of bandwidth. The channel sounder has an absolute timing reference signal sent over the air, which does not limit the transmission distance as a VNA-based channel sounder would since no cable is required to connect the transmitter (Tx) and receiver (Rx).
- We collect the first dataset for broadband MIMO channel sounding results over the 140-160 GHz band in a practical indoor setting.<sup>1</sup>
- Our data analysis indicates that 28.5% of the tested scenarios can support spatial multiplexing. Further, even in cases where spatial multiplexing is not feasible, the

This work was funded by NSF grants CNS-2139930 and CNS-1955004 and the Spanish Ministry of Economic Affairs and Digital Transformation under European Union NextGeneration-EU projects TSI-063000-2021-59 RISC-6G and TSI-063000-2021-63 MAP-6G.

<sup>1</sup>The dataset is available for interested researchers upon request

MIMO channel capacity substantially outperforms the SISO case.

In Sec. II, we describe the experimental platform in detail before explaining how the data is analyzed in Sec. III. The results are presented in Sec. IV, and then we give concluding remarks in Sec. V.

## II. EXPERIMENTAL PLATFORM AND PROCEDURE

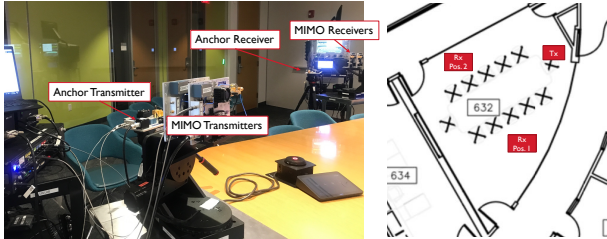


Fig. 1: Test set-up for the experiment. Position 2 is shown on the left.

Enhancing the TeraNova testbed, explained extensively in [6], we build upon its capabilities to perform MIMO channel sounding at sub-THz frequencies. The experimental platform and set-up are shown in Fig. 1 while the block diagram of our system is shown in Fig. 2. The transmission distance for Rx Position 1 is 2.8 m, and for Rx Position 2 it is 3.7 m. The key difference between our platform and other correlation-based channel sounders is that we capture all signals with a LoS reference signal. (From now on, we refer to the LoS reference Tx and Rx pair as the “anchor” and the pair used for true channel sounding as the “MIMO” front-ends.) This reference allows us to determine the relative time-of-arrival information for received signals in addition to the angle-of-arrival information. Using an over-the-air channel for the anchor as opposed to a cable enables us to reach farther distances than VNA-based channel sounders. To ensure no interference between the anchor and the MIMO channel sounding sequence, we operate the anchor front-ends at a lower center frequency (115 GHz) and with a smaller bandwidth (10 GHz) compared with MIMO front-ends, which use 20 GHz of bandwidth centered at 150 GHz. The symbol rate is equal to half of the bandwidth, thus these correspond to symbol rates of 5 GHz and 10 GHz respectively, as shown in Fig. 2. For ease of processing, we keep the overall length of the anchor and MIMO channel sounding sequences the same by using an m-sequence that is half as long for the anchor. The signals are generated in MATLAB and radiated from the TeraNova as detailed in [7].

The anchor generates our reference signal and therefore is stationary throughout the measurements. Meanwhile, front-ends used for MIMO channel sounding are mounted on rotating tables. We measured the channel sweeping each Rx from  $-60^\circ$  to  $60^\circ$ , where  $0^\circ$  corresponds to the perfectly aligned LoS case. Thus, after sweeping each Tx and Rx and capturing the channel sounding and anchor signals, we are

able to calculate the MIMO channel matrix as a function of frequency for any combination of Tx and Rx orientations.

Similar to the approach in [4] and [3], we activate one MIMO Tx/Rx at a time and capture the channel-sounding sequence at each angle with respect to the same LoS reference. More specifically, we follow the procedure below:

- 1) Establish anchor LoS reference path and  $0^\circ$  MIMO path
- 2) Capture the signal while sending the m-sequences from the anchor and first MIMO Tx and sweeping the angle of the Rx from  $-60^\circ$  to  $+60^\circ$
- 3) Rotate the Tx  $10^\circ$  and repeat 2
- 4) Continue until the Tx has swept  $-60^\circ$  to  $+60^\circ$
- 5) Repeat 2 through 4 with the first MIMO Tx and the second MIMO Rx
- 6) Repeat 2 through 4 with the second MIMO Tx and the first MIMO Rx.
- 7) Repeat 2 through 4 with the second MIMO Tx and the second MIMO Rx.

This approach allows us to fully characterize any orientation of the transmitters and receivers. Although we use horn antennas in our analysis, these antennas have comparable gain and directionality to state-of-the-art steerable arrays at the same frequency [8]. Thus, our approach allows us to emulate the array of subarrays architecture that has been put forward for THz MIMO systems [9].

It is also important to note that we used a reference clock to remove any frequency offset between the transmitters and receivers. Additionally, although we rotated the front-ends mechanically, all captures were taken when the hardware was stationary, so the phase shift observed by the Rx should correspond solely to the transmission distance (i.e., no Doppler shift or hardware-introduced phase offset). In other words, the channel is time-invariant, which was validated by observing multiple received signals over time. However, this methodology can and will be used to measure time-varying channels in future work.

## III. BROADBAND MIMO CHANNEL ANALYSIS

From the captured data, we are able to extract the full characteristics of the  $2 \times 2$  MIMO channel for any combination of Tx and Rx orientations. The post-processing for this analysis is displayed in the top right portion of Fig. 2. In the calibration step, we compensate for the hardware response of the hardware components to ensure we are measuring the channel response and not the response of our specific hardware. After calibration, we bring the IF signals to baseband and cross-correlate them with the baseband equivalent of the transmitted m-sequences. At this point, we have preliminary versions of the channel impulse response (CIR) that correspond to the arrival of the anchor and channel-sounding signals. We then shift these CIRs such that the anchor signal is always at  $\tau = 0$ . Then, we remove noise introduced by the m-sequence, the effects of pulse-shaping, and the gain introduced by the m-sequence. The result is the CIR for the given single-input single-output (SISO) channel.

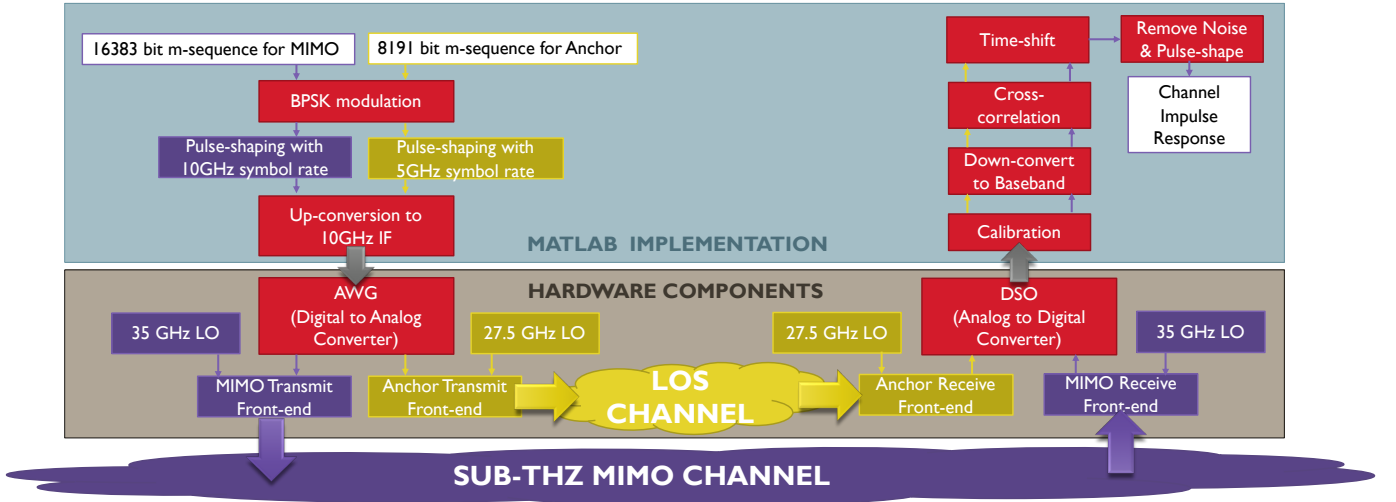


Fig. 2: Test set-up for the experiment. Position 2 is shown on the left.

Taking the Fourier transform, we have the channel transfer function. To find the matrix for any MIMO channel, we place the corresponding SISO transfer functions into a matrix. Thus, we also have the MIMO channel matrix as a function of frequency. Between the channel matrix and the channel impulse responses of each possible channel, we are able to calculate any desired parameters.

#### A. K-factor

In traditional lower-frequency MIMO systems, multi-path propagation is leveraged to ensure that the channels between different antennas are sufficiently varied to enable spatial multiplexing. The Ricean K-factor is essentially a measure of the multi-path propagation of a channel. A high K-factor corresponds to a strictly LoS channel while a low K-factor corresponds to only non-LoS components. Using the time reference provided by the anchor signal in our system, we were able to sum the power of the delay spread related to the LoS path and divide it by the power of the delay spread related to non-LoS paths to find the K-factor. Thus our analysis follows the expression:

$$K[dB] = 10 \log \left( \frac{\sum_{n=i+1}^j P_{Rx}(n)}{\sum_{n=1}^i P_{Rx}(n) + \sum_{n=j+1}^{L_r} P_{Rx}(n)} \right), \quad (1)$$

where  $P_{Rx}(\tau) = |h(\tau)|^2$  is the channel impulse response and  $\tau$  is the time variable.  $i$  is the time instance where the first LoS path arrives at the Rx, and  $j$  corresponds to the time instance of the last LoS arrival.  $L_r$  is the total length of the channel impulse response vector.

#### B. Condition Number

Although a high K-factor indicates a primarily LoS channel, it does not necessarily negate the potential for spatial multiplexing. There have been many works recently discussing LoS MIMO for (sub-)THz systems [10]. The channel condition number provides a better indication of whether spatial multiplexing is feasible. Low condition numbers, ideally below

10 dB, indicate that spatial multiplexing is feasible [11]. The condition number can be calculated directly from the MIMO channel matrix by finding the ratio of the largest to the smallest singular value [11] as

$$CN[dB] = 10 \log \left( \frac{\sigma_{max}}{\sigma_{min}} \right). \quad (2)$$

It is also important to note that, since the channel matrix is a function of frequency, the condition number is also a function of frequency. Therefore for a given scenario, within the studied bandwidth of 20 GHz, there could be parts of the spectrum that are able to support spatial multiplexing while other parts are not. For this reason, in the remainder of this paper, when we refer to the condition number of the channel, we are referring to the worst (maximum) condition number found after calculating the condition number as a function of frequency over the broadband channel.

#### C. Capacity

The capacity of the MIMO system is calculated according to the Shannon limit taking into account water-filling. We use the expression [12]:

$$C_{MIMO} = \Delta f \sum_{f=0}^B \log \left| I_{M_r} + \frac{P_{MIMOopt}(f) \cdot (H_{MIMO}(f) \cdot H_{MIMO}(f)^H)}{N_0 \Delta f M_t} \right|, \quad (3)$$

where  $\Delta f$  is the system's resolution in frequency.  $M_t$  and  $M_r$  are the numbers of transmit and receive antennas respectively.  $P_{MIMOopt}(f)$  is a matrix with the optimal power for each MIMO channel at the frequency  $f$  according to water-filling.  $H_{MIMO}(f)$  is the channel matrix at frequency  $f$ .  $N_0$  is the noise power spectral density. Here,  $\cdot$  represents element-wise multiplication while  $\cdot$  represents matrix multiplication.

## IV. RESULTS

Using the described processes above, we are able to fully characterize the measured sub-THz MIMO channel.

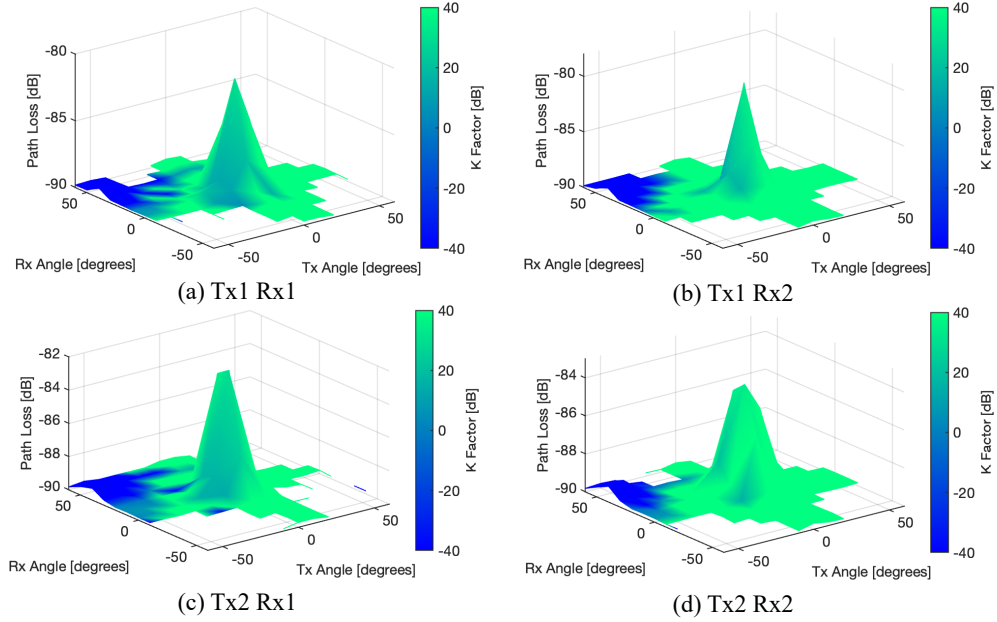


Fig. 3: K factor and path loss of measured SISO channels for Position 1.

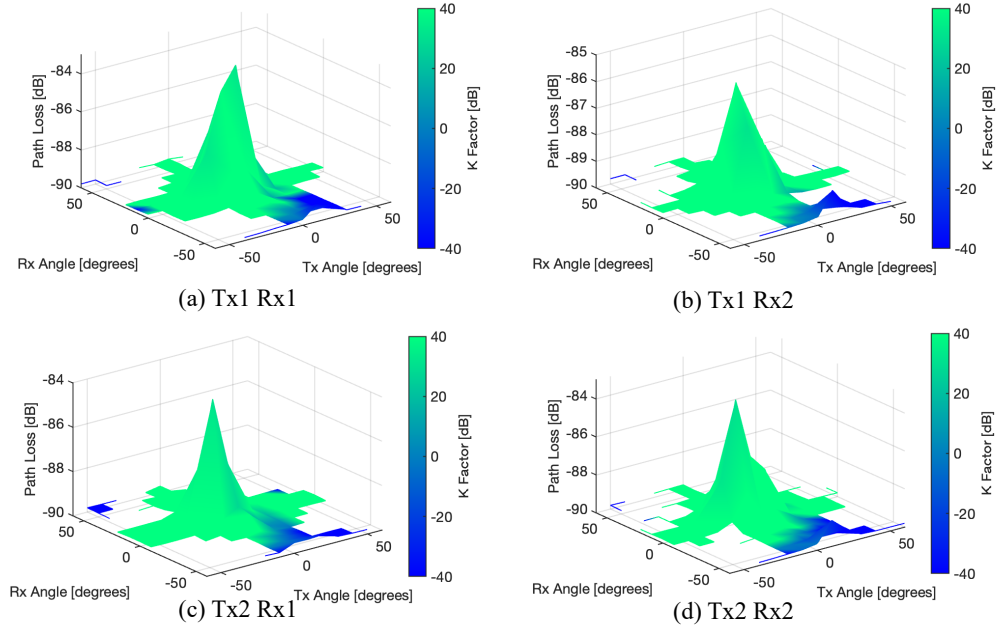


Fig. 4: K factor and path loss of measured SISO channels for Position 2.

#### A. K Factor and Path Loss for each SISO Channel

We start by considering the K factor and path loss, which is displayed in Fig. 3 and Fig. 4 for Rx Positions 1 and 2 respectively. Each subplot corresponds to a measured SISO channel. The angle of the Tx is displayed on the x-axis, while the angle of the Rx is on the y-axis. The color scale corresponds to the K factor, with high K factors (i.e., primarily LoS channels) in green and low K factors (i.e., multi-path channels) in blue. White areas indicate no observed path between the Tx and the

Rx. The z-axis displays the experienced path loss.

We make the following key observations from these plots. First, **the LoS channel is broad**. In the experiments, we use horn antennas with a 3dB beamwidth of  $12^\circ$ , and yet we still observe a LoS component when the difference in angle between Rx and Tx is  $60^\circ$  or even  $70^\circ$ . The gain of our horn antennas is 21 dB; this means that outside of the  $12^\circ$  beamwidth, the antenna still applies up to an 18 dB gain to any incoming or outgoing signal. This observation contradicts

the traditional assumption of ultra-directional transmissions in the THz and sub-THz bands. It is indeed true that THz and sub-THz communications should be directional in many cases, but the existence of such a broad LoS path may motivate more consideration. This phenomenon could adversely affect THz networks in some cases where there is a reliance on directionality to eliminate interference, but it could make neighbor discovery, beam alignment, and the overall performance of a single link more reliable.

Second, we notice that **non-LoS paths do exist**. As corroborated by other studies [13] [14], there can be non-LoS components in a (sub-)THz communication channel. The dark blue section of the plots in Fig. 3 and Fig. 7 indicate a strong LoS component. We see one consistently in the corner corresponding to a Tx angle around  $-50^\circ$  and an Rx angle around  $50^\circ$  for position 1. It is the result of a reflection of a glass wall, and as expected, it moves to the opposite corner in position 2. We also see more sporadic non-LoS components most often observed along with the LoS component, closer to  $0^\circ$ . Although a multi-path channel is not necessarily required for spatial multiplexing, it can be helpful in creating sufficiently different channels to enable spatial multiplexing.

Lastly, we observe that **the channel differs between positions**, both between position 1 and position 2 of the entire MIMO Rx, but also the MIMO Rx1 and MIMO Rx2 (separated by 6 cm) observe different channels. These differences imply that a more comprehensive experimental study should be done to fully characterize the performance of the MIMO channel in more environments, positions, and scenarios.

### B. Condition Number and SNR for each MIMO Channel Matrix

Although the K factor indicates the level of multi-path propagation in a channel, it does not necessarily indicate whether or not the channel is conducive to spatial multiplexing. MIMO channel matrices with low condition numbers are able to support spatial multiplexing. In Fig. 5 we show all the possible MIMO orientations in terms of the average SNR (on the y-axis) and condition number (on the x-axis). The ideal channel for spatial multiplexing will have a high SNR and a low condition number. For Position 1, we see that although 81% of the Tx and Rx orientations would not support spatial multiplexing, 19% of the orientations would, as shown in Fig. 5a. For Position 2, in Fig. 5b, the orientations capable of spatial multiplexing are 38%. Thus considering both positions together, **28.5% of scenarios support spatial multiplexing. Otherwise, beamforming would be the preferred implementation.**

To further explore scenarios where spatial multiplexing is feasible, we also display the condition number and average SNR for a given pair of transmit angles as a function of the Rx angles. In Fig. 6, we show for Tx 1 oriented at  $0^\circ$  degrees and Tx 2 oriented at  $10^\circ$ , the SNR along the z-axis and condition number on the color scale for different Rx orientations. In this scenario, we see a high-SNR-low-condition-number com-

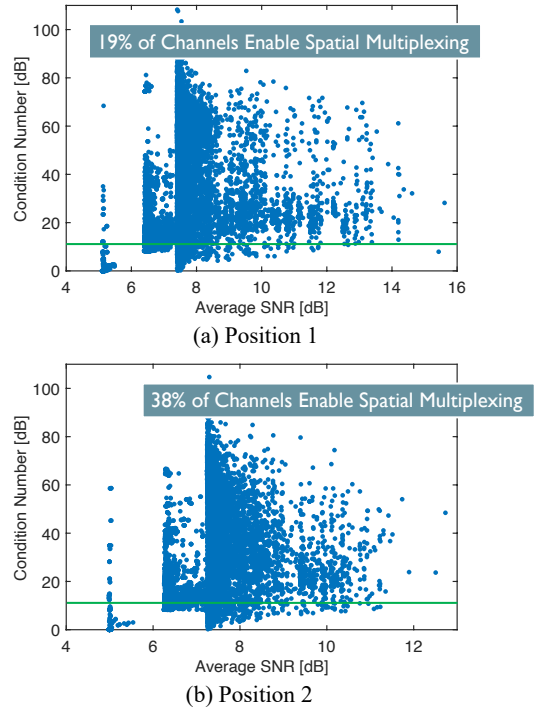


Fig. 5: All MIMO orientations plotted according to the channel matrix’s average SNR and condition number. We consider spatial multiplexing enabled for condition numbers less than 12 dB.

ination when both receivers are oriented at  $0^\circ$ , which again verifies that spatial multiplexing is feasible in LoS scenarios, although it will likely require perfect channel knowledge and may face challenges for mobile systems.

As another example, we include Fig. 7 from Position 2 with Tx 1 oriented at  $30^\circ$  degrees and Tx 2 oriented at  $60^\circ$ . In this case, we see several sets of Rx orientations that correspond to low condition numbers and moderate SNRs. Thus these scenarios could be conducive to spatial multiplexing. Another important note is that the measured SNR is not inherent to the channel. The SNR could be improved in some systems by using higher gain antennas, less noisy hardware components, or a higher power transmitter.

### C. Capacity of the MIMO Channel

Finally, we present the capacity of the measured MIMO channels according to Eq. 3. The results in Fig. 8b show capacities up to 200 Gbps, which is expected using Shannon’s expression for capacity with an average SNR of about 15 dB over 20 GHz of bandwidth with 2 spatially multiplexed channels. Few MIMO combinations lead to the 200 Gbps channel, but there are still many combinations that enable capacities well over 100 Gbps. Considering the capacity jointly with the condition number, as shown in Fig. 8a, we see that many high capacities correspond to low condition numbers, but even in channels with high condition numbers, the capacity can still

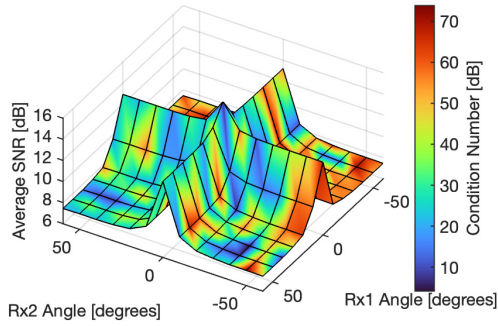


Fig. 6: Tx1 Angle 0 degrees — Tx 2 Angle 10 degrees

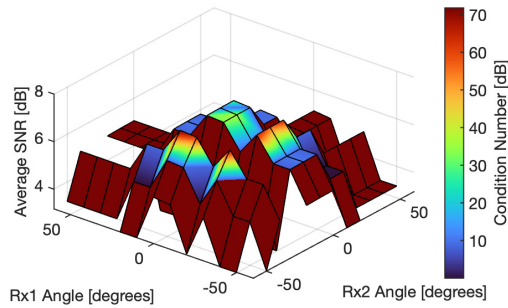
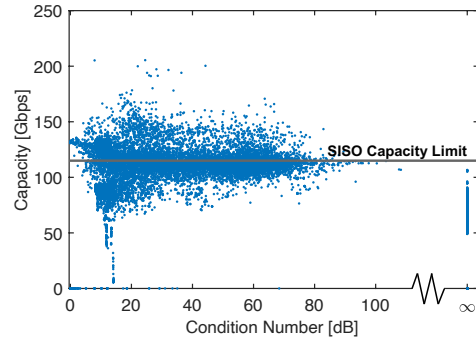
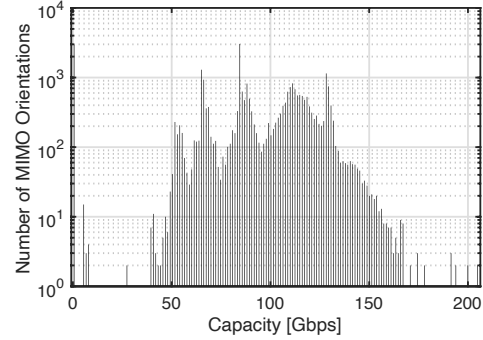


Fig. 7: Tx1 Angle 30 degrees — Tx 2 Angle 60 degrees



(a) Condition Number v. MIMO Capacity Scatter Plot



(b) Histogram of all MIMO orientations

Fig. 8: MIMO Capacity for Rx position 1

be very – and perhaps even just as – high. (In these cases, it is important to recall that capacities will depend both on the channel’s ability to support spatial multiplexing and on the SNR.) In the interest of brevity, we have not included the plots for position 2. Nevertheless, they closely resemble position 1, with a slight decrease in capacity due to the extended transmission distance.

## V. CONCLUSION

In this paper, we present a first-of-its-kind MIMO sub-THz channel sounder to advance the research and development of sub-THz MIMO channel models and experimental solutions. The developed platform enables multiple types of practical analysis involving absolute timing reference. In addition, We showcase preliminary results from a practical indoor setting, and the analysis demonstrates the feasibility of broadband MIMO systems for sub-THz communications. Specifically, we find that spatial multiplexing is feasible in some scenarios, and that sub-THz MIMO systems substantially outperform their SISO counterparts.

## REFERENCES

- [1] M. Polese *et al.*, “Coexistence and Spectrum Sharing Above 100 GHz,” *arXiv preprint arXiv:2110.15187*, 2021.
- [2] C. Han *et al.*, “Terahertz wireless Channels: A Holistic Survey on Measurement, Modeling, and Analysis,” *IEEE Communications Surveys & Tutorials*, vol. 24, no. 3, pp. 1670–1707, 2022.
- [3] H. Xu *et al.*, “Virtual Antenna Array Based Wideband THz MIMO Channel Measurement,” in *2021 IEEE MTT-S International Microwave Workshop Series on Advanced Materials and Processes for RF and THz Applications (IMWS-AMP)*, 2021, pp. 222–224.
- [4] C.-L. Cheng *et al.*, “Terahertz MIMO Fading Analysis and Doppler Modeling in a Data Center Environment,” in *2020 14th European Conference on Antennas and Propagation (EuCAP)*. IEEE, 2020, pp. 1–5.
- [5] S. Rey *et al.*, “Channel Sounding Techniques for Applications in THz Communications: A First Correlation Based Channel Sounder for Ultra-wideband Dynamic Channel Measurements at 300 GHz,” in *2017 9th International Congress on Ultra Modern Telecommunications and Control Systems and Workshops (ICUMT)*. IEEE, 2017, pp. 449–453.
- [6] P. Sen *et al.*, “The TeraNova Platform: An Integrated Testbed for ultra-broadband Wireless Communications at True Terahertz Frequencies,” *Computer Networks*, vol. 179, p. 107370, 2020.
- [7] P. Sen, J. Hall *et al.*, “Terahertz Communications Can Work in Rain and Snow: Impact of Adverse Weather Conditions on Channels at 140 GHz,” in *Proceedings of the 6th ACM Workshop on Millimeter-Wave and Terahertz Networks and Sensing Systems*, 2022, pp. 13–18.
- [8] Abu-Surra *et al.*, “End-to-end 140 GHz Wireless Link Demonstration with Fully-Digital Beamformed System,” in *2021 IEEE International Conference on Communications Workshops (ICC Workshops)*. IEEE, 2021, pp. 1–6.
- [9] C. Lin and G. Y. L. Li, “Terahertz Communications: An Array-of-subarrays Solution,” *IEEE Communications Magazine*, vol. 54, no. 12, pp. 124–131, 2016.
- [10] N. Maletic *et al.*, “A Study of LOS MIMO for Short-Range Sub-THz Wireless Links,” in *Mobile Communication-Technologies and Applications; 25th ITG-Symposium*. VDE, 2021, pp. 1–6.
- [11] S. Schindler and H. Mellein, “Assessing a MIMO channel,” *Rohde & Schwarz white paper, Tech. Rep*, 2011.
- [12] A. Goldsmith, *Wireless Communications*. Cambridge university press, 2005.
- [13] S. Ju and T. S. Rappaport, “Sub-terahertz Spatial Statistical MIMO Channel Model for Urban Microcells at 142 GHz,” in *2021 IEEE Global Communications Conference (GLOBECOM)*. IEEE, 2021, pp. 1–6.
- [14] S. Tarboush *et al.*, “TeraMIMO: A Channel Simulator for Wideband Ultra-Massive MIMO Terahertz Communications,” *IEEE Transactions on Vehicular Technology*, vol. 70, no. 12, pp. 12 325–12 341, 2021.